



HAL
open science

Bcl-2 binds to and inhibits ryanodine receptors.

Tim Vervliet, Elke Decrock, Jordi Molgó, Vincenzo Sorrentino, Ludwig Missiaen, Luc Leybaert, Humbert de Smedt, Nael Nadif Kasri, Jan B Parys, Geert Bultynck

► **To cite this version:**

Tim Vervliet, Elke Decrock, Jordi Molgó, Vincenzo Sorrentino, Ludwig Missiaen, et al.. Bcl-2 binds to and inhibits ryanodine receptors.. *Journal of Cell Science*, 2014, 127 (Pt 12), pp.2782-92. <10.1242/jcs.150011>. <hal-01178836>

HAL Id: hal-01178836

<https://hal.science/hal-01178836v1>

Submitted on 6 Jan 2025

HAL is a multi-disciplinary open access archive for the deposit and dissemination of scientific research documents, whether they are published or not. The documents may come from teaching and research institutions in France or abroad, or from public or private research centers.

L'archive ouverte pluridisciplinaire **HAL**, est destinée au dépôt et à la diffusion de documents scientifiques de niveau recherche, publiés ou non, émanant des établissements d'enseignement et de recherche français ou étrangers, des laboratoires publics ou privés.



HAL Authorization

Bcl-2 binds to and inhibits ryanodine receptors

Tim Vervliet¹, Elke Decrock², Jordi Molgó³, Vincenzo Sorrentino⁴, Ludwig Missiaen¹, Luc Leybaert², Humbert De Smedt¹, Nael Nadif Kasri⁵, Jan B. Parys¹, Geert Bultynck¹

Affiliations

1 KU Leuven, Laboratory of Molecular and Cellular Signaling, Department of Cellular and Molecular Medicine, B-3000 Leuven, Belgium

2 University of Ghent, Physiology Group, Department Basic Medical Sciences, B-9000 Ghent, Belgium

3 Institut de Neurobiologie Alfred Fessard, CNRS, Laboratoire de Neurobiologie et Développement, 91198-Gif sur Yvette cedex, France

4 University of Siena, Molecular Medicine Section, Department of Molecular and Developmental Medicine, and Interuniversity Institute of Myology, 53100 Siena, Italy

5 Donders Institute for Brain, Radboud University Medical Center Cognition and Behaviour, Department of Cognitive Neuroscience, 6500HB Nijmegen, The Netherlands

Corresponding author:

Name: Geert Bultynck

Address: Laboratory of Molecular and Cellular Signaling,
Department of Cellular and Molecular Medicine, KU Leuven
Campus Gasthuisberg, O&N I Herestraat 49 - bus 802, B-3000 Leuven
Belgium

e-mail: geert.bultynck@med.kuleuven.be

Telephone: +32 16 330215

25 **Summary**

26 The anti-apoptotic B-cell lymphoma-2 (Bcl-2) protein not only counteracts apoptosis at
27 the mitochondria by scaffolding pro-apoptotic Bcl-2-family members, but also acts at
28 the endoplasmic reticulum, thereby controlling intracellular Ca^{2+} dynamics. Bcl-2
29 inhibits Ca^{2+} release by targeting the inositol 1,4,5-trisphosphate receptor (IP₃R).
30 Sequence analysis revealed that the Bcl-2-binding site on the IP₃R displays strong
31 homology with a conserved sequence present in all three ryanodine-receptor (RyR)
32 isoforms. We now report that, Bcl-2 co-immunoprecipitated with RyRs in ectopic
33 expression systems and in native rat hippocampi, indicating the existence of
34 endogenous RyR/Bcl-2 complexes. Purified RyR domains containing the putative Bcl-
35 2-binding site bound full-length Bcl-2 in pull-down experiments and interacted with
36 Bcl-2's BH4 domain in surface-plasmon-resonance experiments, suggesting a direct
37 interaction. Exogenous expression of full-length Bcl-2 or electroporation loading of
38 Bcl-2's BH4-domain dampened RyR-mediated Ca^{2+} release in HEK293 cell models.
39 Finally, introducing the BH4-domain peptide into hippocampal neurons via a patch
40 pipette decreased RyR-mediated Ca^{2+} release. In conclusion, this study identifies Bcl-2
41 as a novel inhibitor of RyR-based intracellular Ca^{2+} -release channels.

42 **Keywords**

43 Ca^{2+} signaling, Bcl-2, ryanodine receptor, hippocampus

44 **Introduction**

45 The B-cell lymphoma-2 (Bcl-2) family of proteins consists of both anti- and pro-
46 apoptotic family members. For exerting their function, Bcl-2-family members depend
47 on the presence of one or more Bcl-2-homology (BH) domains (Letai, 2008). The role
48 of anti-apoptotic Bcl-2 proteins, which contain four BH domains, as critical gate
49 keepers of mitochondrial outer-membrane integrity, has been well established (Brunelle
50 and Letai, 2009; Chipuk and Green, 2008). This is achieved by scaffolding and
51 neutralizing pro-apoptotic proteins like Bax/Bak and BH3-only proteins via the
52 hydrophobic cleft, which is formed by the BH3, BH1 and BH2 domains. It has become
53 increasingly clear that Bcl-2 proteins also modulate intracellular Ca^{2+} -signaling events
54 by directly targeting Ca^{2+} -transport mechanisms at different cellular locations. At the
55 level of the endoplasmic reticulum (ER), the main intracellular Ca^{2+} store, Bcl-2-family
56 members target the inositol 1,4,5-trisphosphate (IP_3) receptor (IP_3R) (Monaco et al.,
57 2012a; Oakes et al., 2005; Rong et al., 2008; White et al., 2005), sarco/endoplasmic-
58 reticulum Ca^{2+} -ATPases (SERCA) (Kuo et al., 1998) and Bax inhibitor 1 (BI-1) (Ahn et
59 al., 2010; Xu and Reed, 1998). At the mitochondrial outer membranes, Bcl-2 proteins
60 target the voltage-dependent anion channels (VDAC) (Arbel and Shoshan-Barmatz,
61 2010; Arbel et al., 2012; Plotz et al., 2012). More recently, Bcl-2 was shown to regulate
62 plasma-membrane Ca^{2+} -ATPase (PMCA) activity (Ferdek et al., 2012). Therefore, Bcl-
63 2's function in cells seems to be tightly linked to its ability to modulate intracellular
64 Ca^{2+} homeostasis and dynamics. This is important, given the central role of both Bcl-2
65 and of Ca^{2+} signaling in cell-fate decisions, mitochondrial bio-energetics, autophagy,
66 ER stress and apoptosis (Chipuk et al., 2010; Giorgi et al., 2008; Kiviluoto et al., 2013).
67 Now, recent evidence indicates that the regulation of intracellular Ca^{2+} handling by Bcl-
68 2-family proteins is also important for non-apoptotic functions, including
69 neuroplasticity, cellular migration, cell-cycle regulation and embryonic development
70 (Bonneau et al., 2013).

71 The molecular determinants underlying IP_3R /Bcl-2-complex formation have been
72 identified (Rong et al., 2009; Rong et al., 2008). The BH4 domain of Bcl-2 has been
73 shown to be responsible for binding to a stretch of 20 amino acids located in the central,
74 modulatory domain of the IP_3R . Moreover, Lys17, located in Bcl-2's BH4 domain,

75 seemed important for its binding to the IP₃R and for regulating IP₃R-mediated Ca²⁺
76 release. Lys17 corresponds to Asp11 in the BH4 domain of Bcl-XL and this divergence
77 underlies a striking functional difference between the BH4-domain biology of Bcl-2 and
78 Bcl-XL in inhibiting IP₃R channels and subsequent Ca²⁺ signaling (Monaco et al.,
79 2012b). Sequence analysis of this Bcl-2-binding site on the IP₃R revealed a significant
80 resemblance to a highly conserved stretch of 22 amino acids present in the ryanodine-
81 receptor (RyR) channels, the other major class of tetrameric intracellular Ca²⁺-release
82 channels (Lanner et al., 2010).

83 Guided by this remarkable sequence homology, we now show that Bcl-2, via its BH4
84 domain, directly targets RyR channels in both ectopic expression systems and native rat
85 hippocampi, thereby inhibiting RyR-mediated Ca²⁺ release in RyR-expressing cell
86 models as well as in hippocampal neurons.

87

88 **Results**

89 ***Bcl-2 interacts with RyR channels in HEK293 cell models and in rat hippocampal***
90 ***brain lysates***

91 The Bcl-2-binding site located in the central modulatory domain of the IP₃R (a.a. 1389-
92 1408 for mouse IP₃R1) is well characterized (Rong et al., 2008). This binding site
93 shows great similarity with a region located in the central part of the RyR (a.a. 2448-
94 2469 for rabbit RyR1). Since IP₃Rs and RyRs share several binding partners important
95 for their regulation, it is plausible that Bcl-2 also affects RyR function. In order to verify
96 this, a co-immunoprecipitation approach in HEK293 cells stably overexpressing either
97 RyR1 or RyR3 (HEK RyR1 and HEK RyR3 respectively) was first set up. In these
98 clonal cell lines, RyR levels and endogenous Bcl-2 expression were assessed (Fig. 1A).
99 RyR1 protein-expression levels were lower compared to RyR3 in their respective cell
100 lines. The RyR antibody also detected a stable breakdown product of RyR1 and RyR3
101 resulting in a double signal in the RyR-stained immunoblot as described previously
102 (Xiao et al., 2002). Interestingly, overexpressing either RyR1 or RyR3 respectively
103 induced a 2.36 ± 0.30 and 2.77 ± 0.45 (averages \pm s.d.) fold increase of endogenous
104 Bcl-2-protein levels in comparison to the HEK cells stably expressing the empty vector
105 (HEK mock). Immunoprecipitation of either RyR3 from HEK RyR3 cells (Fig. 1B) or
106 RyR1 from HEK RyR1 cells (Fig. 1C) resulted in the co-immunoprecipitation of
107 endogenous Bcl-2 (lanes 1-2) as well as of transiently overexpressed 3XFLAG-Bcl-2
108 (lanes 3-4). We previously described that the Bcl-2^{K17D} mutant displayed much weaker
109 binding to the regulatory domain of the IP₃R than wild-type Bcl-2 (Monaco et al.,
110 2012b). Yet, 3XFLAG-Bcl-2^{K17D} still co-immunoprecipitated with both RyR3 and
111 RyR1 proteins (Fig. 1D and E). Next, we examined whether endogenous RyR/Bcl-2
112 complexes were present *in vivo*. Hence, lysates from rat hippocampi, which express all
113 three known RyR isoforms, with RyR2 being the most abundantly expressed isoform
114 (Martin et al., 1998; Sharp et al., 1993), were prepared. In these lysates, Bcl-2 co-
115 immunoprecipitated with the endogenous RyRs using the pan-RyR antibody, indicating
116 the presence of endogenous RyR/Bcl-2-protein complexes (Fig. 1F).

117

118

119 ***Bcl-2 targets the central domain of the different RyR isoforms via its BH4 domain***

120 The previous experiments established that Bcl-2 is found in RyR-protein complexes, but
121 neither clarified whether Bcl-2 directly binds to RyR channels nor identified the
122 molecular determinants underlying this interaction. Therefore, we exploited the
123 previously gained insights into the domains of IP₃R and Bcl-2 responsible for
124 IP₃R/Bcl-2-complex formation (Monaco et al., 2012a; Monaco et al., 2012b; Rong et
125 al., 2009). Fig. 2A shows the sequence comparison between the different IP₃R and RyR
126 isoforms, focusing on the known Bcl-2-binding site on the IP₃R (Rong et al., 2008).
127 RyR-protein domains covering approximately 400 a.a. of the central region and
128 containing the putative Bcl-2-binding site on RyR1, RyR2 and RyR3 (a.a. 2404-2827
129 for RyR1 (rabbit), a.a. 2369-2794 for RyR2 (rabbit) and a.a. 2263-2688 for RyR3
130 (mink)) were cloned, expressed and purified as recombinant GST-fusion proteins. The
131 different purified GST-RyR domains were used in GST-pull-down assays, in
132 combination with cell lysates from COS-1 cells transiently overexpressing 3XFLAG-
133 Bcl-2 (Fig. 2B). The previously characterized domain 3 of the IP₃R1 was used as a
134 positive control (Rong et al., 2009). 3XFLAG-Bcl-2 was pulled down by the IP₃R1
135 domain as well as by the different RyR domains (Fig. 2B). The binding of 3xFLAG-
136 Bcl-2 to the purified GST-RyR domains was consistently higher than its binding to GST
137 (Supplementary Fig. 1). These data suggest that Bcl-2 interacts with all three RyR
138 isoforms via a binding site that is located in the central domain of the RyRs.

139 To assess whether Bcl-2 is able to directly bind to the purified RyR domains and clarify
140 whether this binding occurs via Bcl-2's BH4 domain, we performed surface-plasmon-
141 resonance (SPR) experiments. In addition, these data allow for a more quantitative
142 assessment of the RyR/Bcl-2 interaction. In these experiments, the binding of the
143 purified GST-RyR domains to a biotinylated version of Bcl-2's BH4 domain was
144 monitored. All signals were corrected for background binding to a biotinylated
145 scrambled BH4 peptide immobilized to another channel on the same chip. Purified
146 GST-IP₃R1 domain 3 (the positive control) and the respective GST-RyR domains were
147 used as analytes. A concentration-dependent increase in resonance units (RU) indicated
148 a specific binding to biotin-BH4-Bcl-2 for the GST-IP₃R1 domain 3 as well as for the
149 various GST-RyR domains (Fig. 2C, D). Purified GST did not show significant binding

150 to the BH4 domain of Bcl-2 (Fig. 2C). In all cases, the dissociation of the IP₃R and RyR
151 domains from biotin-BH4-Bcl-2 was very slow. Fitted concentration-response curves
152 (Fig. 2D) were determined and used to obtain approximated EC₅₀ values (Table 1). The
153 EC₅₀ value for GST-IP₃R1 domain 3 (0.38 μM) was very similar to those obtained for
154 GST-RyR2 domain (0.38 μM) and GST-RyR3 domain (0.37 μM). Only, the binding of
155 the GST-RyR1 domain seemed to display a lower affinity (EC₅₀ value of 1.53 μM).
156 This indicated that the BH4 domain of Bcl-2 bound to the RyR2 and RyR3 with nearly
157 similar affinities as to IP₃R1, while the affinity of Bcl-2 binding to RyR1 was lower.
158 Given that the binding of Bcl-2 to GST-IP₃R1 domain 3 is critically dependent on the
159 presence of Lys17, we also monitored the binding of the different GST-RyR domains to
160 the biotin-BH4-Bcl-2^{K17D} mutant. The binding of wild-type BH4-Bcl-2 and BH4-Bcl-
161 2^{K17D} to each GST-fusion protein were compared (Fig. 3) and the obtained EC₅₀ values
162 are presented in Table 1. In agreement with our previous findings (Monaco et al.,
163 2012b), binding of the GST-IP₃R1 domain to biotin-BH4-Bcl-2^{K17D} was severely
164 compromised in comparison to biotin-BH4-Bcl-2. In contrast, the binding of the GST-
165 RyR domains was either not affected (in the case of RyR1) or only slightly affected (in
166 the case of RyR2 and RyR3).

167 Collectively, these data indicate that Bcl-2, via its BH4 domain, directly binds to a
168 central region in all three RyR isoforms. Although the BH4 domain was found to be
169 responsible for binding to both the RyR and the IP₃R, the molecular determinants for
170 binding to the RyR were not identical to those for binding to IP₃Rs.

171

172 ***Bcl-2 overexpression inhibits RyR-mediated Ca²⁺ release***

173 We next set out to identify possible functional effects of the Bcl-2-RyR interaction. We
174 performed single-cell [Ca²⁺] measurements to assess the ability of full-size Bcl-2 to
175 inhibit RyR-mediated Ca²⁺ release in a cellular environment. The empty pCMV24
176 vector, a 3XFLAG-Bcl-2-or a 3XFLAG-Bcl-2^{K17D}-containing vector was co-transfected
177 with an mCherry-expressing plasmid in HEK RyR3 cells. Fura-2-AM was used as a
178 cytosolic Ca²⁺ indicator in mCherry-positive cells. All these [Ca²⁺] measurements were
179 performed in the presence of an extracellular Ca²⁺ chelator (BAPTA) in order to study

180 intracellular Ca^{2+} -release events. Caffeine concentrations (1.5 mM) generating sub-
181 maximal responses in these cells were used to induce RyR-mediated Ca^{2+} releases. A
182 typical experiment showing averaged calibrated single-cell $[\text{Ca}^{2+}]$ traces of Fura-2-
183 loaded HEK RyR3 cells expressing the empty vector, 3XFLAG-Bcl-2 or 3XFLAG-Bcl-
184 2^{K17D} is shown in Fig. 4A. Overall, overexpression of 3XFLAG-Bcl-2 or 3XFLAG-Bcl-
185 2^{K17D} inhibited the caffeine-induced Ca^{2+} release by about 30% compared to the empty-
186 vector control in (Fig. 4B). The ER Ca^{2+} -store content was measured by blocking
187 SERCA using 1 μM thapsigargin in the presence of extracellular BAPTA and assessing
188 the total amount of Ca^{2+} released from the stores (area under the curve). These results
189 are summarized in Fig. 4C and indicate that overexpression of 3XFLAG-Bcl-2 or
190 3XFLAG-Bcl- 2^{K17D} did not significantly affect the ER Ca^{2+} -store content in these cells.
191 Similar findings were obtained by overexpressing Bcl-2 or the Bcl- 2^{K17D} mutant in HEK
192 RyR1 cells (Supplementary Fig. 2). Because RyR1-expression levels were slightly
193 lower compared to RyR3 (Fig. 1A) and it was previously reported that, in contrast to the
194 HEK RyR3 cells, these HEK RyR1 cells are less sensitive to stimulation with caffeine
195 (Rossi et al., 2002) a higher concentration of caffeine (4.5 mM) was used to obtain
196 adequate sub-maximal responses.

197 To verify whether the caffeine-induced Ca^{2+} release was dependent on the RyR, similar
198 experiments were also performed using HEK mock cells lacking RyRs. Contrary to the
199 HEK RyR3 cells, administering caffeine did not generate a Ca^{2+} response in HEK mock
200 cells (Fig. 4D). Addition of 2 μM ionomycin resulted, however, in a rise in cytosolic
201 $[\text{Ca}^{2+}]$ in both cell lines, showing that the lack of a caffeine response in HEK mock cells
202 was due to the absence of RyRs. The ionomycin response was lower in the HEK RyR3
203 cells due to a partial depletion of the ER Ca^{2+} pool generated by the caffeine response
204 prior to the addition of ionomycin.

205 Since Bcl-2 is known to inhibit IP_3Rs and Ca^{2+} release from IP_3Rs can activate RyRs via
206 Ca^{2+} -induced Ca^{2+} release, we wanted to exclude that Bcl-2's inhibitory effect on the
207 caffeine-induced Ca^{2+} release occurred via an indirect effect on the IP_3R . To completely
208 exclude this possibility, $[\text{Ca}^{2+}]$ measurements were performed in HEK RyR3 cells in the
209 presence of 2 μM xestospongin B (XeB), an IP_3R inhibitor (Jaimovich et al., 2005).
210 Overexpression of 3XFLAG-Bcl-2 remained equally potent in inhibiting caffeine-

211 induced Ca^{2+} release in RyR3-expressing HEK cells in the presence of XeB (and thus
212 absence of IP_3R activity) (Fig. 4E, F). Since Bcl-2 inhibits RyR-mediated Ca^{2+} release
213 in the presence of a pharmacological IP_3R inhibitor and since the Bcl-2^{K17D} mutant is
214 equally potent in inhibiting RyR-mediated Ca^{2+} release as wild-type Bcl-2, we postulate
215 that the Bcl-2-mediated inhibition of caffeine-induced Ca^{2+} release is due to an
216 inhibition of the RyRs and is not a result of inhibition of IP_3Rs or altered ER-store
217 content.

218 ***The BH4 domain of Bcl-2 is sufficient to inhibit RyR-mediated Ca^{2+} release in HEK***
219 ***RyR3 cells***

220 The single-cell [Ca^{2+}] measurements indicated that the RyR/Bcl-2 interaction inhibits
221 RyR-mediated Ca^{2+} release. In addition, the SPR data (Fig. 2) showed that the Bcl-
222 2/RyR interaction occurs at least in part via the BH4 domain of Bcl-2. We next wanted
223 to identify whether the BH4 domain of Bcl-2 is sufficient to inhibit RyR channels.
224 Hence, we measured RyR-mediated Ca^{2+} release in Fluo-3-loaded HEK RyR3 cells
225 loaded with different concentrations of BH4-Bcl-2 peptide or a scrambled counterpart
226 (Fig. 5A, B). Entry of the peptide into the cells was mediated by electroporation
227 loading, as previously described (De Vuyst et al., 2008). Compared to the vehicle
228 control, electroporation loading of the cells with BH4-Bcl-2 (20 μM) caused a
229 prominent decrease in the caffeine-induced Ca^{2+} release. Performing the same
230 experiment with the scrambled BH4-Bcl-2 peptide (20 μM) did not alter caffeine-
231 induced Ca^{2+} release (Fig. 5A). Electroporation loading of increasing concentrations of
232 BH4-Bcl-2 resulted in a concentration-dependent inhibition of the caffeine-induced
233 Ca^{2+} release, which was not observed utilizing the scrambled BH4-Bcl-2 (Fig. 5B).

234

235 ***The BH4 domain of Bcl-2 inhibits RyR-mediated Ca^{2+} release in hippocampal***
236 ***neuronal cultures***

237 The present data clearly show that the BH4 domain of Bcl-2 is sufficient to bind to and
238 inhibit RyRs. Since these experiments were all performed in cellular models
239 overexpressing RyRs, we next wanted to examine whether the BH4 domain of Bcl-2 is
240 also able to inhibit endogenous RyR channels. Given the presence of endogenous

241 RyR/Bcl-2 complexes in rat hippocampal neurons (Fig. 1F), we opted to study the
242 regulation of RyR channels by the BH4 domain of Bcl-2 in these cells.

243 Dissociated hippocampal neurons were infected at 7 days in vitro (DIV) with an adeno-
244 associated virus expressing GCaMP3. Single-cell $[Ca^{2+}]$ measurements were performed
245 between 14 and 18 DIV. GCaMP3 was used as a genetically encoded fluorescent Ca^{2+}
246 indicator (Yamada and Mikoshiba, 2012). Utilizing whole-cell voltage-clamp, the
247 membrane potential was clamped at -60 mV thereby preventing Ca^{2+} influx from the
248 extracellular space through voltage-gated Ca^{2+} channels. In this way, the measured
249 changes in fluorescence could be attributed to changes in intracellular Ca^{2+} release and
250 were not due to Ca^{2+} influx across the plasma membrane. At the same time the BH4
251 domain of Bcl-2, the scrambled BH4-domain peptide or the vehicle control (DMSO)
252 were introduced into the neurons via the patch pipette. A scheme of the experimental
253 protocol is provided in Fig. 6A. Local application of 10 mM caffeine resulted in RyR-
254 mediated Ca^{2+} release. Fig. 6B shows representative images from a time-lapse
255 experiment and Fig. 6C shows a typical trace obtained for each condition. Introducing
256 the BH4 domain of Bcl-2 (20 μ M) into the soma of the neurons led to a prominent
257 inhibition of the caffeine-induced Ca^{2+} release compared to introducing either the
258 vehicle (DMSO) control or the scrambled BH4 domain of Bcl-2 in the neurons (Fig.
259 6B-D). Pretreatment of the neurons with 50 μ M ryanodine almost completely blocked
260 caffeine-induced Ca^{2+} release indicating that the observed Ca^{2+} release was attributed to
261 RyR activity (Fig. 6E). Taken together, these data indicate that the BH4 domain of Bcl-
262 2 can inhibit native RyR channels in hippocampal neurons.

263

264 **Discussion**

265 The major finding of this study is that RyR channels, an important class of intracellular
266 Ca^{2+} -release channels, are novel targets for the anti-apoptotic Bcl-2 proteins in both
267 ectopic RyR-expressing cell systems and primary tissues like the hippocampus. We
268 showed that Bcl-2 via its BH4 domain directly binds to the central domain of the RyR
269 channels, thereby suppressing RyR-mediated Ca^{2+} release. These findings clearly
270 underpin the emerging role for Bcl-2 proteins in intracellular Ca^{2+} signaling by directly
271 targeting an increasing number of Ca^{2+} -transporting systems at intracellular and
272 plasmalemmal membranes, including IP₃Rs (Hanson et al., 2008; Rong et al., 2009;
273 Rong et al., 2008), SERCA (Kuo et al., 1998), VDAC (Arbel and Shoshan-Barmatz,
274 2010), BI-1 (Ahn et al., 2010; Xu and Reed, 1998) and PMCA (Ferdek et al., 2012).

275 The binding of Bcl-2 to the RyR shows a striking resemblance with the binding of Bcl-2
276 to the IP₃R. The latter is interesting because IP₃Rs and RyRs show many similarities at
277 both the structural and functional level (Furuichi et al., 1994; Seo et al., 2012). Both
278 intracellular Ca^{2+} -release channels are modulated by the same cellular factors like Ca^{2+} ,
279 ATP and Mg^{2+} (Bezprozvanny et al., 1991; Bull et al., 2007; Dias et al., 2006; Maes et
280 al., 2001; Mak and Foskett, 1998). In addition, several kinases target both channels e.g.
281 PK (protein kinase) A, PKC, PKG and Ca^{2+} /calmodulin-dependent protein kinase II
282 (Furuichi et al., 1994; Lanner et al., 2010; Vanderheyden et al., 2009). Different
283 regulatory proteins interact with both the IP₃Rs and the RyRs. Calmodulin for example
284 regulates the Ca^{2+} sensitivity of IP₃Rs (Kasri et al., 2004) and RyRs (Balshaw et al.,
285 2001). Our data now clearly indicate that, in a similar way as for the IP₃R (Rong et al.,
286 2008), RyRs are also targets of Bcl-2. Importantly, the RyRs contain a sequence that has
287 approximately 60% homology to the Bcl-2-binding site located in the central,
288 modulatory region of IP₃Rs (Rong et al., 2008). Bcl-2 binds to this site on the IP₃R
289 through its BH4 domain (Rong et al., 2009). Our results (Fig. 2) indicate a similar
290 behavior for Bcl-2 with respect to the RyRs. This similarity extends to the functional
291 level as binding of the BH4 domain of Bcl-2 leads in both IP₃Rs (Rong et al., 2009) and
292 RyRs to a suppression of channel-mediated Ca^{2+} release.

293 Sequence alignment revealed a 22 a.a. spanning region (a.a. 2309-2330, mink RyR3) in
294 the RyR that displays striking homology with the known Bcl-2-binding site of the IP₃R.

295 In addition, the proposed region is highly conserved across all RyR isoforms of
296 different species. It can be anticipated that regulation of RyRs by Bcl-2 is important, as
297 the proposed Bcl-2-binding site on the RyR is already known to be a crucial regulatory
298 site for RyR-channel stability. Structural coupling (RyR zipping) of this centrally
299 located site to the N-terminus is critical for adequate RyR functioning (Ikemoto and
300 Yamamoto, 2002; Yamamoto and Ikemoto, 2002). Disruption of this interaction (RyR
301 unzipping) generates leaky RyR channels and triggers irregular channel activity. This
302 central site is also part of a mutational hotspot in RyR1 and RyR2 involved in the onset
303 of malignant hyperthermia (Hwang et al., 2012) or arrhythmia (Yano, 2008),
304 respectively. Structural information about this mutational hotspot has been obtained
305 from 3D cryo-EM studies. In an elegant study, a green fluorescent protein (GFP) tag
306 was introduced at residue 2367 of RyR2 (Liu et al., 2005), about 60 amino acids
307 upstream of the here described Bcl-2-binding site. The location of the GFP insert was
308 mapped to a bridge area between domain 5 and domain 6 (Liu et al., 2005). This area is
309 known to be located at the cytoplasmic face of the RyR (Radermacher et al., 1994).
310 Thus, we anticipate that the region where the Bcl-2-binding site is located should be
311 accessible for interaction.

312 In addition, a proposed binding site for the 12-kDa and 12.6-kDa FK506-binding
313 proteins (FKBP12 and FKBP12.6) on the different RyR isoforms is located within the
314 binding domain for Bcl-2 on the RyRs identified in this study (Brillantes et al., 1994;
315 Bultynck et al., 2001b; Gaburjakova et al., 2001; Marx et al., 2000; Van Acker et al.,
316 2004). Both FKBP12 and FKBP12.6 are immunophilins tightly associated with the
317 RyR, necessary for stabilizing the channel (Brillantes et al., 1994). In this way, these
318 proteins inhibit excessive Ca^{2+} leak via RyRs. Since Bcl-2 targets a site in close
319 proximity to a FKBP12/FKBP12.6-binding site, it is not surprising that Bcl-2 binding to
320 RyRs elicits functional consequences. It remains to be determined whether the binding
321 of immunophilins and Bcl-2-family proteins compete for the same, similar or
322 overlapping sites and whether RyR/Bcl-2 complexes are present in tissues containing
323 high levels of FKBP12/FKBP12.6, such as skeletal and cardiac muscle. In any case,
324 further experiments are needed, since additional FKBP12/FKBP12.6-binding sites on
325 RyR channels have been proposed. More specifically, for the cardiac RyR2 channel,
326 FKBP12.6 has been described to bind to both an N-terminal site (Masumiya et al.,

2003) and a C-terminal site (Zissimopoulos and Lai, 2005a; Zissimopoulos and Lai, 2005b). Further experiments investigating competition between Bcl-2 and FKBP12/FKBP12.6 for the binding to the different RyR isoforms may therefore provide additional insights in these apparent discrepancies. Furthermore, we previously reported that despite sequence similarities between the proposed FKBP12-binding site on IP₃R_s and RyR_s, their properties and secondary structure may be different (Bultynck et al., 2001a; Bultynck et al., 2001b). Hence, these differences may contribute to the fact that in IP₃R_s this site preferentially binds Bcl-2 over the Bcl-2^{K17D} mutant, whereas for the equivalent site in the RyR_s there was a nearly similar binding of Bcl-2 and Bcl-2^{K17D}. Finally, other factors such as ATP may also influence Bcl-2 binding to the RyR as the proposed site for Bcl-2 binding in RyR_s has also been implicated in ATP binding (Blayney et al., 2013; Zissimopoulos and Lai, 2005b).

The role of RyR_s in cell-survival and cell-death decisions is much less well documented than for the IP₃R. RyR_s however can similarly as IP₃R_s, also mediate Ca²⁺ signaling into mitochondria (Hajnoczky et al., 2002). The exact molecular mechanisms of this Ca²⁺ transfer to the mitochondria remain poorly understood. A recent paper showed that VDAC2 is coupled to RyR2 in the heart (Min et al., 2012), allowing a direct coupling of RyR-mediated Ca²⁺ release to Ca²⁺ uptake in the mitochondria. Moreover, RyR-mediated Ca²⁺ signaling has been implicated in ATP production and metabolic flexibility in the heart (Broun et al., 2013). Other studies implicated RyR_s in the regulation of apoptosis (Kim et al., 2002) and ER stress-mediated cell death (Luciani et al., 2009; Ruiz et al., 2009) in various cell types, including neurons and pancreatic β cells. The Bcl-2/RyR interaction described here could therefore provide an important regulatory mechanism by which RyR activity controls cell fate. Further studies will be needed to unravel the exact cell biological and/or physiological role of Bcl-2 binding to RyR_s in cell-fate decisions and functions beyond apoptosis. It is becoming increasingly clear that Ca²⁺ signaling and RyR_s play important roles in memory formation and neurodegenerative diseases (Berridge, 2013; Berridge, 2011). The presence of RyR/Bcl-2 complexes in the hippocampus (Fig. 1F) and the observation that the BH4 domain of Bcl-2 is able to inhibit RyR-mediated Ca²⁺ release in hippocampal neurons (Fig. 6), may suggest that Bcl-2, via regulating RyR channels, has an important function in the brain.

359 In conclusion, we identified RyR channels as novel cellular targets for anti-apoptotic
360 Bcl-2 proteins. Our findings show that Bcl-2 targets and regulates the two main families
361 of intracellular Ca²⁺-release channels, IP₃Rs and RyRs, in a similar way. This further
362 strengthens the role of Bcl-2 proteins as essential regulators of Ca²⁺-signaling events
363 and places RyR channels in the growing list of Ca²⁺-transport systems that are targeted
364 by Bcl-2.

365

391 Reverse: 5'GCGGCGGAATTCCTATCGGGTTCTTTCAATCCTCC3'
392 RyR3 Forward: 5'GCGGCGGGATCCAAGAGAGAAGTCATGGAGGACGG3'
393 Reverse: 5'GCGGCGGAATTCCTATTTGGTCCTCTCCACAGACC3'

394 *Protein purification*

395 GST-fusion-protein purification was performed as described previously (Bultynck et al.,
396 2001b) except for the induction of protein synthesis, which was performed with 0.1 mM
397 isopropyl β -d-thiogalactoside for 20 hours at 14°C. After the purification, dialysis and
398 handling of the proteins was performed as described (Monaco et al., 2012b).

399 *Cell culture and transfections*

400 All media and supplements added to the medium used in this paper were purchased
401 from Life Technologies (Ghent, Belgium). HEK293 cells stably expressing an empty
402 pcDNA3.1(-) vector (HEK mock) or stably overexpressing RyR1 or RyR3 (Rossi et al.,
403 2002) were cultured at 37°C in a 5% CO₂ incubator in α -Minimum Essential Medium
404 supplemented with 10% fetal calf serum, 100 IU/ml penicillin, 100 μ g/ml streptomycin,
405 2 mM glutamax and 800 μ g/ml G418. COS-1 cells were cultured in Dulbecco's
406 Modified Eagle's medium, containing 10% fetal calf serum, 100 IU/ml penicillin, 100
407 μ g/ml streptomycin, 2.5 μ g/ml fungizone and 2 mM glutamax at 37°C, 10% CO₂.

408 One day after seeding, cells were transiently transfected with either empty p3XFLAG-
409 Myc-CMV-24 or with the same vector containing Bcl-2 or Bcl-2^{K17D}. JETprime
410 transfection reagent (Polyplus Transfections, Illkirch, France) was used according to the
411 manufacturer's instruction. Two days later, HEK mock, HEK RyR1 or HEK RyR3 cells
412 were harvested and lysed using a CHAPS-based lysis buffer (pH 7.5, 50 mM Tris-HCl,
413 100 mM NaCl, 2 mM EDTA, 50 mM NaF, 1 mM Na₃VO₄, 1% CHAPS and protease
414 inhibitor tablets (Roche, Basel, Switzerland)). For COS-1 cells a Triton X-100 based
415 lysis buffer (pH 7.5, 25 mM HEPES, 100 mM NaCl, 1.5 mM MgCl₂, 0.5 mM DTT,
416 10% glycerol, 1% Triton X-100 and protease inhibitor tablets) was used. Cells for
417 [Ca²⁺] measurements were seeded in 2-chamber slides and transfected two days later
418 using the X-tremeGENE HP DNA transfection reagent (Roche) according to the

419 manufacturer's protocol. As a selection marker pcDNA 3.1(-) mCherry vector was co-
420 transfected at a 1:3 ratio to the p3XFLAG-Myc-CMV-24 vectors.

421 *Dissociated hippocampal cultures*

422 Dissociated hippocampal neurons were prepared as described previously (Nadif Kasri et
423 al., 2011). Briefly, embryonic day 18 rat hippocampi were dissected and washed with
424 ice-cold Hanks' balanced salt solution (HBSS) without Mg^{2+} or Ca^{2+} (Life
425 Technologies) supplemented with 10 mM HEPES at pH 7.3. Following a 15 min
426 incubation with 0.25% trypsin at 37°C, the hippocampi were again washed with the
427 HBSS solution. After removing the last wash, seeding medium (neurobasal medium
428 containing 10% FBS, 100 IU/ml penicillin, 100 μ g/ml streptomycin and 2% B27
429 supplement) was added. Using polished Pasteur pipettes the hippocampi were
430 dissociated and seeded on polyethylene-treated cover slips at 50000 cells/coverslip.
431 Four hours later, half of the seeding medium was replaced with culturing medium
432 (neurobasal medium containing 2 mM glutamax, 100 IU/ml penicillin, 100 μ g/ml
433 streptomycin and 2% B27 supplement). Half of the medium was replaced with culturing
434 medium every three days.

435 *GST-pull downs*

436 The purified GST-fusion proteins or parental GST (0.5 μ M) were incubated in the
437 Triton X-100 lysis buffer together with 70 μ g of COS-1-cell lysates overexpressing the
438 3XFLAG-Bcl-2 protein (final volume 500 μ l). The incubation was performed at 4°C
439 using a head-over-head rotator. After 1 hour, the GST-fusion proteins were immobilized
440 to glutathione-Sepharose® 4B beads (GE Healthcare, Diegem, Belgium). 1.5 to 2 hours
441 later, the Sepharose beads were washed 5 times using Triton X-100 lysis buffer.
442 Subsequently, the complexes were eluted in 40 μ l 2X LDS (Life Technologies)
443 supplemented with 1/200 β -mercaptoethanol for 5 min at 95°C. Ten μ l of the collected
444 eluate was used for immunoblot analysis. GelCode Blue (Thermo Scientific) was used
445 to determine the total amount of protein present on the PVDF membrane (Millipore,
446 Billerica, MA, USA). For quantification, the amount of 3XFLAG-Bcl-2 bound to the
447 different GST-fusion proteins was divided by the amount of GST-tagged protein present

448 on the membrane corrected for their difference in molecular mass. Values are presented
449 relative to the amount bound to the positive control, GST-IP₃R1 domain 3.

450 *SPR analysis*

451 SPR analysis was performed using a Biacore T100 (GE Healthcare). Immobilization to
452 the streptavidin-coated sensor chip (BR-1005-31; GE Healthcare) and SPR
453 measurements were performed as described previously (Monaco et al., 2012b). NaOH
454 (50 mM) with 0.0026% SDS was used as a regeneration buffer. Dose-response curves
455 were fitted using the Hill equation. For comparing the binding of the GST-tagged
456 domains to the wild-type BH4-Bcl-2 and the BH4-Bcl-2^{K17D} mutant, the V_{max} of the
457 fitted curves was fixed to the estimated value for the wild-type BH4 domain for each
458 GST-fusion domain.

459 *Co-immunoprecipitation experiments*

460 A co-immunoprecipitation kit (Thermo Scientific) was used. Five µg of either the RyR
461 antibody or a mouse IgG control antibody was covalently immobilized to 20 µl of the
462 resin according to the manufacturers' protocol except for the final washing step, which
463 was performed using the CHAPS-based lysis buffer. Next, when using lysates of cells
464 overexpressing RyRs and 3XFLAG-Bcl-2 proteins, 200 µg of pre-cleared cell lysate
465 was incubated overnight at 4°C in CHAPS lysis buffer together with the resin
466 containing the antibody. For detection of interactions with endogenous Bcl-2 in the
467 RyR-overexpressing HEK cells, 400 µg of cell lysate was used without prior pre-
468 clearing. The next day, the resin was washed 4-5 times with CHAPS lysis buffer, after
469 which the elution was performed by boiling the samples for 5 min at 95°C in 50 µl of
470 2X LDS supplemented with 1/200 β-mercaptoethanol. Twenty-one day-old rat
471 hippocampi were homogenized in the CHAPS lysis buffer and incubated for 30 min at
472 4°C. After centrifugation (4000xg) the supernatant was used for co-
473 immunoprecipitation of endogenous Bcl-2/RyR complexes. The same protocol was
474 used as for the co-immunoprecipitations in the HEK RyR cells with endogenous Bcl-2
475 with the exception that, the amount of washes was reduced to two.

476

477 ***Immunoblot analysis***

478 Samples were prepared and used as previously described (Monaco et al., 2012b). For
479 visualization of RyRs, NuPAGE 3-8% Tris acetate gels were run. Detection was
480 performed using Pierce ECL Western Blotting Substrate (Thermo Scientific). For
481 developing, either CL-Xposure Films (Thermo Scientific) were used in combination
482 with an X-OMAT 1000 processor (Kodak, Zaventem, Belgium) or a Chemidoc™ MP
483 system (Bio Rad, Nazareth Eke, Belgium).

484 ***Electroporation loading and Ca²⁺ imaging***

485 HEK RyR3 cells were grown as adherent monolayers to near confluency on 18 mm-
486 diameter glass coverslips. Cell cultures were ester-loaded for 45 min with 10 μM Fluo-
487 3-AM (Life Technologies) in HBSS with Ca²⁺ and Mg²⁺ (Life Technologies)
488 supplemented with 25 mM HEPES (HBSS-HEPES) and 0.01% pluronic F-127 (Life
489 Technologies) at room temperature, followed by de-esterification for 15 min.
490 Subsequently, a fine narrow zone of cells was loaded with Bcl-2 peptides and the
491 fluorescent dye Dextran TEXAS Red (100 μM; Life Technologies) using an *in situ*
492 electroporation technique, as described previously (De Vuyst et al., 2008; Decrock et
493 al., 2009; Monaco et al., 2012b). Briefly, cells were rinsed three times with HBSS-
494 HEPES followed by three washes with a low conductivity electroporation buffer (4.02
495 mM KH₂PO₄, 10.8 mM K₂HPO₄, 1.0 mM MgCl₂, 300 mM sorbitol, 2.0 mM HEPES,
496 pH 7.4). The cells were positioned 400 μm underneath a two-wire Pt-Ir electrode on the
497 microscopic stage and electroporated in the presence of a tiny amount of electroporation
498 solution (10 μl). Electroporation was performed with 50 kHz bipolar pulses at a field
499 strength of 2000 V/cm and applied as 15 trains of 10 pulses of 2 msec duration each.
500 After electroporation, cells were thoroughly washed with HBSS-HEPES and left 5 min
501 to recover before proceeding with the Ca²⁺ imaging. For the latter, cells were superfused
502 for 1 min with HBSS-HEPES, followed by 8 min with 1 mM caffeine in HBSS-HEPES.
503 Imaging was carried out using an inverted Nikon Eclipse TE300 fluorescence
504 microscope (Nikon, Brussels, Belgium) equipped with a x40 oil immersion objective
505 and an EM-CCD camera (QuantEM 512SC, Photometrics, Tuscon, AZ, USA). Images
506 (1/sec) were generated with custom-developed FluoFrames software written in

507 Microsoft Visual C++ 6.0. Fluorescence-intensity changes in all cells were analyzed with
508 FluoFrames software. For each individual trace, the relative change of Fluo-3
509 fluorescence $((F-F_0)/F_0)$ was calculated. Subsequently, relative cytoplasmic $[Ca^{2+}]$
510 changes were quantified as the area under the curve of the separate Ca^{2+} traces. Data
511 were normalized to the vehicle (DMSO) condition, which was set as 100%.

512 *Fura-2-AM $[Ca^{2+}]$ measurements*

513 A Zeiss Axio Observer Z1 Inverted Microscope equipped with a 20x air objective and a
514 high-speed digital camera (AxioCam Hsm, Zeiss, Jena, Germany) were used. HEK
515 RyR1 or HEK RyR3 cells co-transfected with 0.133 μ g mCherry and 0.333 μ g of the
516 3XFLAG constructs were loaded, two days after transfection, at room temperature,
517 using Fura-2-AM (1.25 μ M; Biotium, Hayward, CA, USA) in modified Krebs buffer
518 (135 mM NaCl, 6.2 mM KCl, 1.2 mM $MgCl_2$, 12 mM HEPES, pH 7.3, 11.5 mM
519 glucose and 2 mM $CaCl_2$). After 30 min, de-esterification was allowed to occur for 30
520 min at room temperature. Before starting the $[Ca^{2+}]$ measurements, mCherry-positive
521 cells were selected. During the experiment, 3 mM BAPTA (Alfa Aesar, Ward Hill, MA,
522 USA) was added to buffer extracellular Ca^{2+} . Caffeine and thapsigargin (Alomone Labs,
523 Jerusalem, Israel) responses were measured. For calibration, minimal and maximal
524 Fura-2 responses were subsequently determined using 2 μ M of ionomycin (Enzo Life
525 Sciences, Farmingdale, NY, USA) supplemented with 50 mM EGTA or 500 mM $CaCl_2$
526 respectively in modified Krebs buffer. When XeB (2 μ M) was used, it was added to the
527 cell medium one hour prior to Fura-2-AM loading of the cell. XeB was also included
528 during all steps of the loading process. The cytosolic $[Ca^{2+}]$ was calculated using
529 $[Ca^{2+}]$ (nM) = $K_d \times (F_{380max}/F_{380min}) \times (R - R_{min}) / (R_{max} - R)$, where K_d is the dissociation
530 constant of Fura-2 for Ca^{2+} at room temperature (220 nM). In each experiment, 15-20
531 mCherry-positive cells were measured, which was repeated on at least three different
532 days. Maximum peak values were calculated for each calibrated trace by subtracting the
533 baseline $[Ca^{2+}]$ from the maximum response, followed by averaging individual data
534 points. Replicate experiments within the same day were also averaged and used for
535 obtaining final averages for all days. For thapsigargin experiments the area under the
536 curve was determined by integrating the curves from the time point when thapsigargin
537 was added, until calibration was started 10 min later.

538 *Hippocampal [Ca²⁺] measurements*

539 One week before measuring, a genetically encoded GCaMP3 Ca²⁺ indicator was
540 introduced in the neurons via adenoviral infection. 14 to 18 day-old hippocampal
541 neurons were used for these experiments. The cover slips were placed in the perfusion
542 chamber of a Slice Scope microscope (Scientifica, East Sussex, UK). The neurons were
543 perfused with heated (30°C), oxygenated artificial cerebrospinal fluid (aCSF)
544 containing: 124 mM NaCl, 1.25 mM NaH₂PO₄, 3 mM KCl, 26 mM NaHCO₃, 2 mM
545 CaCl₂, 1 mM MgCl₂ and 10 mM glucose at pH 7.4. Tetrodotoxin (1 μM) (Tocris
546 Bioscience, Bristol, UK) was added just before use. Patch pipettes with a 4 MΩ
547 resistance were pulled from borosilicate capillaries (Science Products GmbH, Hofheim,
548 Germany). These were filled with the following solution: 115 mM CsMeSO₃, 20 mM
549 CsCl, 10 mM HEPES, 2.5 mM MgCl₂, 4 mM Na₂-ATP, 0.4 mM Na₂-GTP, 10 mM Na-
550 phosphocreatine and 0.1 mM EGTA. The vehicle (DMSO) or 20 μM of either the
551 scrambled BH4-Bcl-2 or the BH4-Bcl-2 peptide was added to this solution just before
552 the experiment. Utilizing whole-cell voltage clamp the membrane potential was
553 clamped at -60 mV using a MultiClamp 700B amplifier (Molecular Devices, Biberach
554 an der Riss, Germany). After five min of incubation with the peptide the [Ca²⁺]
555 measurement was started. Using a pneumatic drug-ejection system (PDES-02DX from
556 NPI, Tamm, Germany), a local 10 mM caffeine puff was administered after 1 min
557 through a second patch pipette positioned 15-25 μm from the cell. Imaging was
558 performed using a CoolLED pE-2 excitation system (Life Sciences & Analytical,
559 Andover, UK) in combination with an ORCA-Flash2.8 C11440-10C camera
560 (Hamamatsu, Almere, the Netherlands). HImage software (Hamamatsu) was used for
561 analyzing the [Ca²⁺] measurements.

562 *Statistical analysis*

563 When comparing two conditions, two-tailed, unpaired student t-tests were performed.
564 For comparing three or more groups, repeated measure ANOVA with Bonferroni post
565 test was performed. * indicates significantly different results when p<0.05. The exact p-
566 values have been indicated in the figures, where feasible.

567

568 **Acknowledgements**

569 We would like to thank Karol Ondrias and Zuzana Tomaskova for the helpful
570 discussions, and Marco Benevento, Martijn Selten, Wei Ba, Lubica Malekova, Kirsten
571 Welkenhuyzen, Giovanni Monaco, Marina Crabbé and Anja Florizoone for their
572 excellent technical assistance. This work was supported by the Research Foundation-
573 Flanders (FWO) grants. 6.057.12 to GB and LL and G.0134.09N to LL, by the Research
574 Council of the KU Leuven via an OT START grant (STR1/10/044) to GB, by the
575 Interuniversity Attraction Poles Program (Belgian Science Policy; P7/13 to JBP, GB
576 and LM and P7/10 to LL), by the “Donders Center for Neuroscience fellowship award
577 of the Radboud University Nijmegen Medical Center” to NNK and by the “FP7-Marie
578 Curie International Reintegration Grant” to NNK grant number 277091. TV was
579 supported by FWO travel grant V42613N.

580 **The authors declare no competing interests.**

581

582 **References**

- 583 **Ahn, T., Yun, C. H., Kim, H. R. and Chae, H. J.** (2010). Cardiolipin, phosphatidylserine, and
584 BH4 domain of Bcl-2 family regulate $\text{Ca}^{2+}/\text{H}^{+}$ antiporter activity of human Bax inhibitor-1. *Cell*
585 *Calcium*. 47:387-96.
- 586 **Arbel, N. and Shoshan-Barmatz, V.** (2010). Voltage-dependent anion channel 1-based
587 peptides interact with Bcl-2 to prevent antiapoptotic activity. *J Biol Chem*. 285:6053-62.
- 588 **Arbel, N., Ben-Hail, D. and Shoshan-Barmatz, V.** (2012). Mediation of the antiapoptotic
589 activity of Bcl-xL protein upon interaction with VDAC1 protein. *J Biol Chem*. 287:23152-61.
- 590 **Balshaw, D. M., Xu, L., Yamaguchi, N., Pasek, D. A. and Meissner, G.** (2001). Calmodulin
591 binding and inhibition of cardiac muscle calcium release channel (ryanodine receptor). *J Biol*
592 *Chem*. 276:20144-20153.
- 593 **Berridge, M. J.** (2013). Calcium regulation of neural rhythms, memory and Alzheimer's
594 disease. *J Physiol*. Epub ahead of print.
- 595 **Berridge, M. J.** (2011). Calcium signalling and Alzheimer's disease. *Neurochem Res*. 36:1149-
596 56.
- 597 **Bezprozvanny, I., Watras, J. and Ehrlich, B. E.** (1991). Bell-shaped calcium-response curves
598 of $\text{Ins}(1,4,5)\text{P}_3$ - and calcium-gated channels from endoplasmic reticulum of cerebellum. *Nature*.
599 351:751-4.
- 600 **Blayney, L., Beck, K., MacDonald, E., D'Cruz, L., Nomikos, M., Griffiths, J.,**
601 **Thanassoulas, A., Nounesis, G. and Lai, F. A.** (2013). ATP interacts with the CPVT mutation-
602 associated central domain of the cardiac ryanodine receptor. *Biochim Biophys Acta-Gen Subj*.
603 1830:4426-32.
- 604 **Bonneau, B., Prudent, J., Popgeorgiev, N. and Gillet, G.** (2013). Non-apoptotic roles of Bcl-
605 2 family: the calcium connection. *Biochim Biophys-Acta Mol Cell Res*. 1833:1755-65.
- 606 **Brillantes, A. B., Ondrias, K., Scott, A., Kobrinsky, E., Ondriasova, E., Moschella, M. C.,**
607 **Jayaraman, T., Landers, M., Ehrlich, B. E. and Marks, A. R.** (1994). Stabilization of
608 calcium release channel (ryanodine receptor) function by FK506-binding protein. *Cell*. 77:513-
609 23.
- 610 **Bround, M. J., Wambolt, R., Luciani, D. S., Kulpa, J. E., Rodrigues, B., Brownsey, R. W.,**
611 **Allard, M. F. and Johnson, J. D.** (2013). Cardiomyocyte ATP production, metabolic
612 flexibility, and survival require calcium flux through cardiac ryanodine receptors in vivo. *J Biol*
613 *Chem*. 288:18975-86.
- 614 **Brunelle, J. K. and Letai, A.** (2009). Control of mitochondrial apoptosis by the Bcl-2 family. *J*
615 *Cell Sci*. 122:437-41.
- 616 **Bull, R., Finkelstein, J. P., Humeres, A., Behrens, M. I. and Hidalgo, C.** (2007). Effects of
617 ATP, Mg^{2+} , and redox agents on the Ca^{2+} dependence of RyR channels from rat brain cortex.
618 *Am J Physiol Cell Physiol*. 293:C162-71.
- 619 **Bultynck, G., Rossi, D., Callewaert, G., Missiaen, L., Sorrentino, V., Parys, J. B. and De**
620 **Smedt, H.** (2001a). The conserved sites for the FK506-binding proteins in ryanodine receptors
621 and inositol 1,4,5-trisphosphate receptors are structurally and functionally different. *J Biol*
622 *Chem*. 276:47715-24.
- 623 **Bultynck, G., De Smet, P., Rossi, D., Callewaert, G., Missiaen, L., Sorrentino, V., De**
624 **Smedt, H. and Parys, J. B.** (2001b). Characterization and mapping of the 12 kDa FK506-
625 binding protein (FKBP12)-binding site on different isoforms of the ryanodine receptor and of
626 the inositol 1,4,5-trisphosphate receptor. *Biochem J*. 354:413-22.
- 627 **Chipuk, J. E. and Green, D. R.** (2008). How do BCL-2 proteins induce mitochondrial outer
628 membrane permeabilization? *Trends Cell Biol*. 18:157-64.
- 629 **Chipuk, J. E., Moldoveanu, T., Llambi, F., Parsons, M. J. and Green, D. R.** (2010). The
630 BCL-2 family reunion. *Mol Cell*. 37:299-310.
- 631 **De Vuyst, E., De Bock, M., Decrock, E., Van Moorhem, M., Naus, C., Mabilde, C. and**
632 **Leybaert, L.** (2008). In situ bipolar electroporation for localized cell loading with reporter dyes
633 and investigating gap junctional coupling. *Biophys J*. 94:469-79.

634 **Decrock, E., De Vuyst, E., Vinken, M., Van Moorhem, M., Vranckx, K., Wang, N., Van**
635 **Laeken, L., De Bock, M., D'Herde, K., Lai, C. P. et al.** (2009). Connexin 43 hemichannels
636 contribute to the propagation of apoptotic cell death in a rat C6 glioma cell model. *Cell Death*
637 *Differ.* 16:151-63.

638 **Dias, J. M., Szegedi, C., Jona, I. and Vogel, P. D.** (2006). Insights into the regulation of the
639 ryanodine receptor: differential effects of Mg^{2+} and Ca^{2+} on ATP binding. *Biochemistry.*
640 45:9408-15.

641 **Ferde, P. E., Gerasimenko, J. V., Peng, S., Tepikin, A. V., Petersen, O. H. and**
642 **Gerasimenko, O. V.** (2012). A novel role for Bcl-2 in regulation of cellular calcium extrusion.
643 *Curr Biol.* 22:1241-6.

644 **Furuichi, T., Kohda, K., Miyawaki, A. and Mikoshiba, K.** (1994). Intracellular channels.
645 *Curr Opin Neurobiol.* 4:294-303.

646 **Gaburjakova, M., Gaburjakova, J., Reiken, S., Huang, F., Marx, S. O., Rosemlit, N. and**
647 **Marks, A. R.** (2001). FKBP12 binding modulates ryanodine receptor channel gating. *J Biol*
648 *Chem.* 276:16931-5.

649 **Giorgi, C., Romagnoli, A., Pinton, P. and Rizzuto, R.** (2008). Ca^{2+} signaling, mitochondria
650 and cell death. *Curr Mol Med.* 8:119-30.

651 **Hajnoczky, G., Csordas, G. and Yi, M.** (2002). Old players in a new role: mitochondria-
652 associated membranes, VDAC, and ryanodine receptors as contributors to calcium signal
653 propagation from endoplasmic reticulum to the mitochondria. *Cell Calcium.* 32:363-77.

654 **Hanson, C. J., Bootman, M. D., Distelhorst, C. W., Wojcikiewicz, R. J. and Roderick, H. L.**
655 (2008). Bcl-2 suppresses Ca^{2+} release through inositol 1,4,5-trisphosphate receptors and inhibits
656 Ca^{2+} uptake by mitochondria without affecting ER calcium store content. *Cell Calcium.* 44:324-
657 38.

658 **Hwang, J. H., Zorzato, F., Clarke, N. F. and Treves, S.** (2012). Mapping domains and
659 mutations on the skeletal muscle ryanodine receptor channel. *Trends Mol Med.* 18:644-57.

660 **Ikemoto, N. and Yamamoto, T.** (2002). Regulation of calcium release by interdomain
661 interaction within ryanodine receptors. *Front Biosci.* 7:d671-83.

662 **Jaimovich, E., Mattei, C., Liberona, J. L., Cardenas, C., Estrada, M., Barbier, J., Debitus,**
663 **C., Laurent, D. and Molgo, J.** (2005). Xestospongins B, a competitive inhibitor of IP_3 -mediated
664 Ca^{2+} signalling in cultured rat myotubes, isolated myonuclei, and neuroblastoma (NG108-15)
665 cells. *FEBS Lett.* 579:2051-7.

666 **Kasri, N. N., Parys, J. B., Callewaert, G., Missiaen, L. and De Smedt, H.** (2004).
667 Calmodulin and calcium-release channels. *Biol Res.* 37:577-82.

668 **Kim, B. C., Kim, H. T., Mamura, M., Ambudkar, I. S., Choi, K. S. and Kim, S. J.** (2002).
669 Tumor necrosis factor induces apoptosis in hepatoma cells by increasing Ca^{2+} release from the
670 endoplasmic reticulum and suppressing Bcl-2 expression. *J Biol Chem.* 277:31381-9.

671 **Kiviluoto, S., Vervliet, T., Ivanova, H., Decuypere, J. P., De Smedt, H., Missiaen, L.,**
672 **Bultynck, G. and Parys, J. B.** (2013). Regulation of inositol 1,4,5-trisphosphate receptors
673 during endoplasmic reticulum stress. *Biochim Biophys Acta-Mol Cell Res.* 1833:1612-24.

674 **Kuo, T. H., Kim, H. R., Zhu, L., Yu, Y., Lin, H. M. and Tsang, W.** (1998). Modulation of
675 endoplasmic reticulum calcium pump by Bcl-2. *Oncogene.* 17:1903-10.

676 **Lanner, J. T., Georgiou, D. K., Joshi, A. D. and Hamilton, S. L.** (2010). Ryanodine
677 receptors: structure, expression, molecular details, and function in calcium release. *Cold Spring*
678 *Harb Perspect Biol.* 2:a003996.

679 **Letai, A. G.** (2008). Diagnosing and exploiting cancer's addiction to blocks in apoptosis. *Nat*
680 *Rev Cancer.* 8:121-32.

681 **Liu, Z., Wang, R., Zhang, J., Chen, S. R. and Wagenknecht, T.** (2005). Localization of a
682 disease-associated mutation site in the three-dimensional structure of the cardiac muscle
683 ryanodine receptor. *J Biol Chem.* 280:37941-7.

684 **Luciani, D. S., Gwiazda, K. S., Yang, T. L., Kalynyak, T. B., Bychkivska, Y., Frey, M. H.,**
685 **Jeffrey, K. D., Sampaio, A. V., Underhill, T. M. and Johnson, J. D.** (2009). Roles of IP_3R

686 and RyR Ca²⁺ channels in endoplasmic reticulum stress and beta-cell death. *Diabetes*. 58:422-
687 32.

688 **Maes, K., Missiaen, L., Parys, J. B., De Smet, P., Sienaert, I., Waelkens, E., Callewaert, G.**
689 **and De Smedt, H.** (2001). Mapping of the ATP-binding sites on inositol 1,4,5-trisphosphate
690 receptor type 1 and type 3 homotetramers by controlled proteolysis and photoaffinity labeling. *J*
691 *Biol Chem*. 276:3492-7.

692 **Mak, D. O. and Foskett, J. K.** (1998). Effects of divalent cations on single-channel conduction
693 properties of Xenopus IP₃ receptor. *Am J Physiol Cell Physiol*. 275:C179-88.

694 **Martin, C., Chapman, K. E., Seckl, J. R. and Ashley, R. H.** (1998). Partial cloning and
695 differential expression of ryanodine receptor calcium-release channel genes in human tissues
696 including the hippocampus and cerebellum. *Neuroscience*. 85:205-216.

697 **Marx, S. O., Reiken, S., Hisamatsu, Y., Jayaraman, T., Burkhoff, D., Rosemblyt, N. and**
698 **Marks, A. R.** (2000). PKA phosphorylation dissociates FKBP12.6 from the calcium release
699 channel (ryanodine receptor): defective regulation in failing hearts. *Cell*. 101:365-76.

700 **Masumiya, H., Wang, R., Zhang, J., Xiao, B. and Chen, S. R.** (2003). Localization of the
701 12.6-kDa FK506-binding protein (FKBP12.6) binding site to the NH₂-terminal domain of the
702 cardiac Ca²⁺ release channel (ryanodine receptor). *J Biol Chem*. 278:3786-92.

703 **Min, C. K., Yeom, D. R., Lee, K. E., Kwon, H. K., Kang, M., Kim, Y. S., Park, Z. Y., Jeon,**
704 **H. and Kim do, H.** (2012). Coupling of ryanodine receptor 2 and voltage-dependent anion
705 channel 2 is essential for Ca²⁺ transfer from the sarcoplasmic reticulum to the mitochondria in
706 the heart. *Biochem J*. 447:371-9.

707 **Monaco, G., Beckers, M., Ivanova, H., Missiaen, L., Parys, J. B., De Smedt, H. and**
708 **Bultynck, G.** (2012a). Profiling of the Bcl-2/Bcl-X_L-binding sites on type 1 IP₃ receptor.
709 *Biochem Biophys Res Commun*. 428:31-5.

710 **Monaco, G., Decrock, E., Akl, H., Ponsaerts, R., Vervliet, T., Luyten, T., De Maeyer, M.,**
711 **Missiaen, L., Distelhorst, C. W., De Smedt, H. et al.** (2012b). Selective regulation of IP₃-
712 receptor-mediated Ca²⁺ signaling and apoptosis by the BH4 domain of Bcl-2 versus Bcl-X_L. *Cell*
713 *Death Differ*. 19:295-309.

714 **Nadif Kasri, N., Nakano-Kobayashi, A. and Van Aelst, L.** (2011). Rapid synthesis of the X-
715 linked mental retardation protein OPHN1 mediates mGluR-dependent LTD through interaction
716 with the endocytic machinery. *Neuron*. 72:300-15.

717 **Oakes, S. A., Scorrano, L., Opferman, J. T., Bassik, M. C., Nishino, M., Pozzan, T. and**
718 **Korsmeyer, S. J.** (2005). Proapoptotic BAX and BAK regulate the type 1 inositol trisphosphate
719 receptor and calcium leak from the endoplasmic reticulum. *Proc Natl Acad Sci U S A*. 102:105-
720 10.

721 **Plotz, M., Gillissen, B., Hossini, A. M., Daniel, P. T. and Eberle, J.** (2012). Disruption of the
722 VDAC2-Bak interaction by Bcl-x_S mediates efficient induction of apoptosis in melanoma cells.
723 *Cell Death Differ*. 19:1928-38.

724 **Quirion, J. C., Sevenet, T., Husson, H. P., Weniger, B. and Debitus, C.** (1992). Two new
725 alkaloids from Xestospongia sp., a New Caledonian sponge. *J Nat Prod*. 55:1505-8.

726 **Radermacher, M., Rao, V., Grassucci, R., Frank, J., Timerman, A. P., Fleischer, S. and**
727 **Wagenknecht, T.** (1994). Cryo-electron microscopy and three-dimensional reconstruction of
728 the calcium release channel/ryanodine receptor from skeletal muscle. *J Cell Biol*. 127:411-23.

729 **Rong, Y. P., Bultynck, G., Aromolaran, A. S., Zhong, F., Parys, J. B., De Smedt, H.,**
730 **Mignery, G. A., Roderick, H. L., Bootman, M. D. and Distelhorst, C. W.** (2009). The BH4
731 domain of Bcl-2 inhibits ER calcium release and apoptosis by binding the regulatory and
732 coupling domain of the IP₃ receptor. *Proc Natl Acad Sci U S A*. 106:14397-402.

733 **Rong, Y. P., Aromolaran, A. S., Bultynck, G., Zhong, F., Li, X., McColl, K., Matsuyama,**
734 **S., Herlitzte, S., Roderick, H. L., Bootman, M. D. et al.** (2008). Targeting Bcl-2-IP₃ receptor
735 interaction to reverse Bcl-2's inhibition of apoptotic calcium signals. *Mol Cell*. 31:255-65.

736 **Rossi, D., Simeoni, I., Micheli, M., Bootman, M., Lipp, P., Allen, P. D. and Sorrentino, V.**
737 (2002). RyR1 and RyR3 isoforms provide distinct intracellular Ca²⁺ signals in HEK 293 cells. *J*
738 *Cell Sci*. 115:2497-504.

739 **Ruiz, A., Matute, C. and Alberdi, E.** (2009). Endoplasmic reticulum Ca²⁺ release through
740 ryanodine and IP₃ receptors contributes to neuronal excitotoxicity. *Cell Calcium*. 46:273-81.
741 **Seo, M. D., Velamakanni, S., Ishiyama, N., Stathopoulos, P. B., Rossi, A. M., Khan, S. A.,**
742 **Dale, P., Li, C., Ames, J. B., Ikura, M. et al.** (2012). Structural and functional conservation of
743 key domains in InsP₃ and ryanodine receptors. *Nature*. 483:108-12.
744 **Sharp, A. H., Mcpherson, P. S., Dawson, T. M., Aoki, C., Campbell, K. P. and Snyder, S.**
745 **H.** (1993). Differential immunohistochemical localization of inositol 1,4,5-trisphosphate-
746 sensitive and ryanodine-sensitive Ca²⁺ release channels in rat-brain. *J Neurosci*. 13:3051-3063.
747 **Van Acker, K., Bultynck, G., Rossi, D., Sorrentino, V., Boens, N., Missiaen, L., De Smedt,**
748 **H., Parys, J. B. and Callewaert, G.** (2004). The 12 kDa FK506-binding protein, FKBP12,
749 modulates the Ca²⁺-flux properties of the type-3 ryanodine receptor. *J Cell Sci*. 117:1129-37.
750 **Vanderheyden, V., Devogelaere, B., Missiaen, L., De Smedt, H., Bultynck, G. and Parys, J.**
751 **B.** (2009). Regulation of inositol 1,4,5-trisphosphate-induced Ca²⁺ release by reversible
752 phosphorylation and dephosphorylation. *Biochim Biophys Acta-Mol Cell Res*. 1793:959-70.
753 **White, C., Li, C., Yang, J., Petrenko, N. B., Madesh, M., Thompson, C. B. and Foskett, J.**
754 **K.** (2005). The endoplasmic reticulum gateway to apoptosis by Bcl-X_L modulation of the
755 InsP₃R. *Nat Cell Biol*. 7:1021-8.
756 **Xiao, B., Masumiya, H., Jiang, D., Wang, R., Sei, Y., Zhang, L., Murayama, T., Ogawa, Y.,**
757 **Lai, F. A., Wagenknecht, T. et al.** (2002). Isoform-dependent formation of heteromeric Ca²⁺
758 release channels (ryanodine receptors). *J Biol Chem*. 277:41778-85.
759 **Xu, Q. and Reed, J. C.** (1998). Bax inhibitor-1, a mammalian apoptosis suppressor identified
760 by functional screening in yeast. *Mol Cell*. 1:337-46.
761 **Yamada, Y. and Mikoshiba, K.** (2012). Quantitative comparison of novel GCaMP-type
762 genetically encoded Ca²⁺ indicators in mammalian neurons. *Front Cell Neurosci*. 6:41.
763 **Yamamoto, T. and Ikemoto, N.** (2002). Spectroscopic monitoring of local conformational
764 changes during the intramolecular domain-domain interaction of the ryanodine receptor.
765 *Biochemistry*. 41:1492-501.
766 **Yano, M.** (2008). Ryanodine receptor as a new therapeutic target of heart failure and lethal
767 arrhythmia. *Circ J*. 72:509-14.
768 **Zissimopoulos, S. and Lai, F. A.** (2005a). Interaction of FKBP12.6 with the cardiac ryanodine
769 receptor C-terminal domain. *J Biol Chem*. 280:5475-85.
770 **Zissimopoulos, S. and Lai, F. A.** (2005b). Central domain of the human cardiac muscle
771 ryanodine receptor does not mediate interaction with FKBP12.6. *Cell Biochem Biophys*. 43:203-
772 19.
773
774
775

776 **Figure legends**

777

778 **Figure 1. Bcl-2 interacts with both overexpressed and endogenous RyRs**

779 (A) Immunoblot showing the expression of RyRs, Bcl-2 and GAPDH (loading control)
780 in cell lysates from empty vector-expressing HEK cells (HEK mock), RyR1-expressing
781 HEK cells (HEK RyR1) and RyR3-expressing HEK cells (HEK RyR3). (B, C)
782 Immunoblots from co-immunoprecipitation experiments using HEK RyR3 (B) and
783 HEK RyR1 (C) cell lysates. RyR3 or RyR1 was immunoprecipitated using a pan-RyR
784 antibody. Co-immunoprecipitation of endogenous Bcl-2 with RyRs (lanes 1-2) was
785 assessed via immunoblotting using a Bcl-2 antibody. Co-immunoprecipitation of
786 ectopically expressed 3XFLAG-Bcl-2 (lanes 3-4) was assessed via immunoblotting
787 using a FLAG antibody. (D, E lanes 1-2) Similar experiments were performed as in B
788 and C (lanes 3-4) but utilizing the 3XFLAG-Bcl-2^{K17D} mutant. Immunoprecipitations
789 using non-specific IgGs were included for every condition to assess the level of non-
790 specific binding. 0.2 and 0.5 µg of total cell lysate was taken as input for the 3XFLAG-
791 tagged proteins and the RyR, respectively (input). (F) Immunoblots showing a typical
792 co-immunoprecipitation experiment using lysates obtained from 21-day old rat
793 hippocampi. The endogenous RyRs were immunoprecipitated and the presence of
794 endogenous Bcl-2/RyR complexes was assessed using a Bcl-2 antibody. The IgG co-
795 immunoprecipitation was used as negative control. 10 µg of total lysates was used as
796 input. Each experiment was performed at least three times utilizing each time a newly
797 prepared cell or hippocampal lysate. The double lines in panel B to E indicate were two
798 parts of the same immunoblot (and same exposure time) were merged.

799

800 **Figure 2. Bcl-2 binds to RyRs through its BH4 domain**

801 (A) Sequence alignment of the relevant sites on the three mouse IP₃R isoforms (IP₃R1:
802 a.a. 1389-1408, IP₃R2: a.a. 1390-1409, IP₃R3: a.a. 1380-1499) and the three RyR
803 isoforms (rabbit RyR1: a.a. 2448-2469, rabbit RyR2: a.a. 2415-2436, mink RyR3: a.a.
804 2309-2330) based on the known Bcl-2-binding site on the IP₃R. Identical (green) or
805 similar (red) amino acids are indicated. (B) Example of the performed GST-pull-down

806 experiments. Top: GelCode Blue staining of an immunoblot showing total amounts of
807 the pulled-down GST or GST-tagged proteins. Bottom: immunoblot stained with FLAG
808 antibody showing the amounts of pulled-down 3XFLAG-Bcl-2 protein. GST was used
809 as a negative control. 0.1 μg of total COS-1 lysates was used as input. The experiments
810 were repeated at least 5 times using at least 3 different batches of the GST-tagged
811 domains and each time a new COS-1 cell lysate. (C) Representative, background-
812 corrected sensorgrams obtained from SPR experiments in which biotin-BH4-Bcl-2
813 immobilized to streptavidin-coated sensor chips was exposed to GST-tagged proteins
814 (1.1 μM) or GST alone (5 μM). Binding was expressed in resonance units (RU) as a
815 function of time. Binding of the GST-fusion proteins to the biotin-BH4-Bcl-2 was
816 corrected for non-specific binding by subtracting the response of these proteins to the
817 biotin-scrambled BH4 domain loaded in a different channel on the same sensor chip.
818 The first arrow indicates the start of the association phase (addition of the GST-fusion
819 proteins or GST diluted in running buffer), while the second arrow indicates the start of
820 the dissociation phase (running buffer alone). All experiments were performed using
821 different sensor chips and at least three different preparations of the GST-tagged
822 proteins. (D) Averages of the responses to the GST-tagged proteins for each tested
823 concentration were determined and used to fit dose response-curves. For clarity reasons,
824 the fitted curve corresponding to the RyR2 domain is depicted here as a dashed line.
825 Data points indicate averages \pm s.e.m. (n=3).

826

827 **Figure 3. Comparison of biotin-BH4-Bcl-2 and biotin-BH4-Bcl-2^{K17D} for binding to**
828 **the GST-RyR domains**

829 Binding of the different GST-domains to biotin-BH4-Bcl-2 and Biotin-BH4-Bcl-2^{K17D}
830 was compared in SPR experiments similarly performed as in Fig. 2C and D. Biotin-
831 BH4-Bcl-2^{K17D} was immobilized to a different channel on the same sensor chip as
832 biotin-BH4-Bcl-2. Averages of the responses to the GST-tagged proteins for each
833 concentration were determined and plotted for both the wild-type BH4-Bcl-2 and the
834 BH4-Bcl-2^{K17D} mutant. Data points indicate averages \pm s.e.m. (n=3). Estimated EC₅₀
835 values obtained from the fitted dose response-curves are shown in Table 1.

836 **Figure 4. Overexpression of Bcl-2 inhibits RyR-mediated Ca²⁺ release**

837 Fura-2 loaded, transfected (mCherry-positive) HEK RYR3 cells were selected for
838 single-cell [Ca²⁺] measurements. (A) Average calibrated [Ca²⁺] traces (20 cells) from
839 HEK RyR3 cells containing the pCMV24 vector, 3XFLAG-Bcl-2 or 3XFLAG-Bcl-
840 2^{K17D} obtained in one experiment. The administration of BAPTA (3 mM) and caffeine
841 (1.5 mM) is indicated by the arrows. (B) Quantitative analysis of the caffeine responses
842 in HEK RyR3 cells; values show averages ± s.e.m. of at least 4 independent
843 experiments (n>100 cells). (C) Quantitative analysis of the ER Ca²⁺-store content. The
844 ER Ca²⁺-store content was determined similarly as in panel A, except that thapsigargin
845 (1 μM) was used instead of caffeine. The area under the curve (AUC) of the calibrated
846 traces was used for determining the total ER Ca²⁺-store content. The bar graph indicates
847 the average AUC ± s.e.m. of at least 3 independent experiments (n>80 cells) for each
848 condition. (D) Average calibrated [Ca²⁺] traces (20 cells) from HEK mock or HEK
849 RyR3 cells. The administration of caffeine (1.5 mM) and ionomycin (2 μM) is indicated
850 by the arrows. (E) Typical experiment depicting average calibrated [Ca²⁺] traces (20
851 cells) from empty-vector control cells and 3XFLAG-Bcl-2-expressing cells showing
852 caffeine-induced Ca²⁺ release in the presence of 2 μM of the IP₃R inhibitor XeB. The
853 administration of BAPTA (3 mM) and caffeine (1.5 mM) is indicated by the arrows.
854 (F) Quantification of the caffeine responses for each condition in the presence of XeB.
855 Values depict averages of ± s.e.m. of at least 5 independent experiments (n>80
856 cells/condition).

857

858 **Figure 5. The BH4 domain of Bcl-2 is sufficient for inhibiting RyR3-mediated Ca²⁺**
859 **release**

860 Single-cell Fluo-3 [Ca²⁺] measurements were performed in HEK RyR3 cells. The
861 vehicle (DMSO), the BH4 domain of Bcl-2 or the scrambled peptide were loaded via
862 electroporation (10, 20 or 40 μM), after which 1 mM of caffeine was used as stimulus.
863 (A) Typical traces obtained for each condition after electroporation loading with 20 μM
864 of the peptides or the vehicle. The arrow indicates the time where caffeine (1 mM) was
865 added. The traces are represented as (F-F₀)/F₀. (B) Quantitative analysis of all

866 experiments. Averages of 5 independent experiments are given as relative responses \pm
867 s.e.m. compared to the DMSO control. The caffeine responses were normalized to the
868 vehicle control.

869

870 **Figure 6. The BH4 domain of Bcl-2 inhibits RyR-mediated Ca²⁺ release in**
871 **hippocampal neuronal cultures**

872 Single-cell [Ca²⁺] measurements were performed on 14- to 18-day old dissociated
873 hippocampal neuronal cultures. GCaMP3-positive cells were selected for the
874 measurements. The vehicle (DMSO), a scrambled version of the BH4 domain of Bcl-2
875 (20 μ M) or the BH4 domain of Bcl-2 (20 μ M) were introduced into the cell via the
876 patch pipette. At the same time, the membrane potential was clamped at -60 mV. (A)
877 Scheme of the performed experiment starting from the time when whole-cell voltage-
878 clamp was obtained. Caffeine (10 mM) was locally applied via a second patch pipette
879 positioned next to the cell. (B) Time lapse of a typical experiment for each tested
880 condition performed, focusing on the time when caffeine was applied locally. Scale bar,
881 5 μ m. (C) Typical caffeine-induced Ca²⁺-release responses measured in the soma of one
882 neuron for each tested condition. The fluorescence was normalized to the baseline
883 fluorescence and represented as $(F-F_0)/F_0$. The arrow indicates the time point when
884 caffeine was applied. (D) Summary of all performed measurements for the scrambled
885 BH4 domain of Bcl-2 and the BH4 domain of Bcl-2 normalized to the vehicle control.
886 The circles indicate the average of all [Ca²⁺] measurements (2 to 4 cells) performed per
887 condition each day. [Ca²⁺] measurements performed on the same day are indicated in
888 the same color. The average \pm s.e.m. of 6 independent experiments is indicated in black
889 (n=19 cells for each condition). (E) Typical single-cell [Ca²⁺] measurement performed
890 in neurons pretreated for 20 min with either the vehicle (DMSO) (black) or 50 μ M
891 ryanodine (grey). The arrow indicates the time point when caffeine was applied. The
892 fluorescence was normalized to the baseline fluorescence and represented as $(F-F_0)/F_0$.
893 Experiments were performed at least 5 times.

894

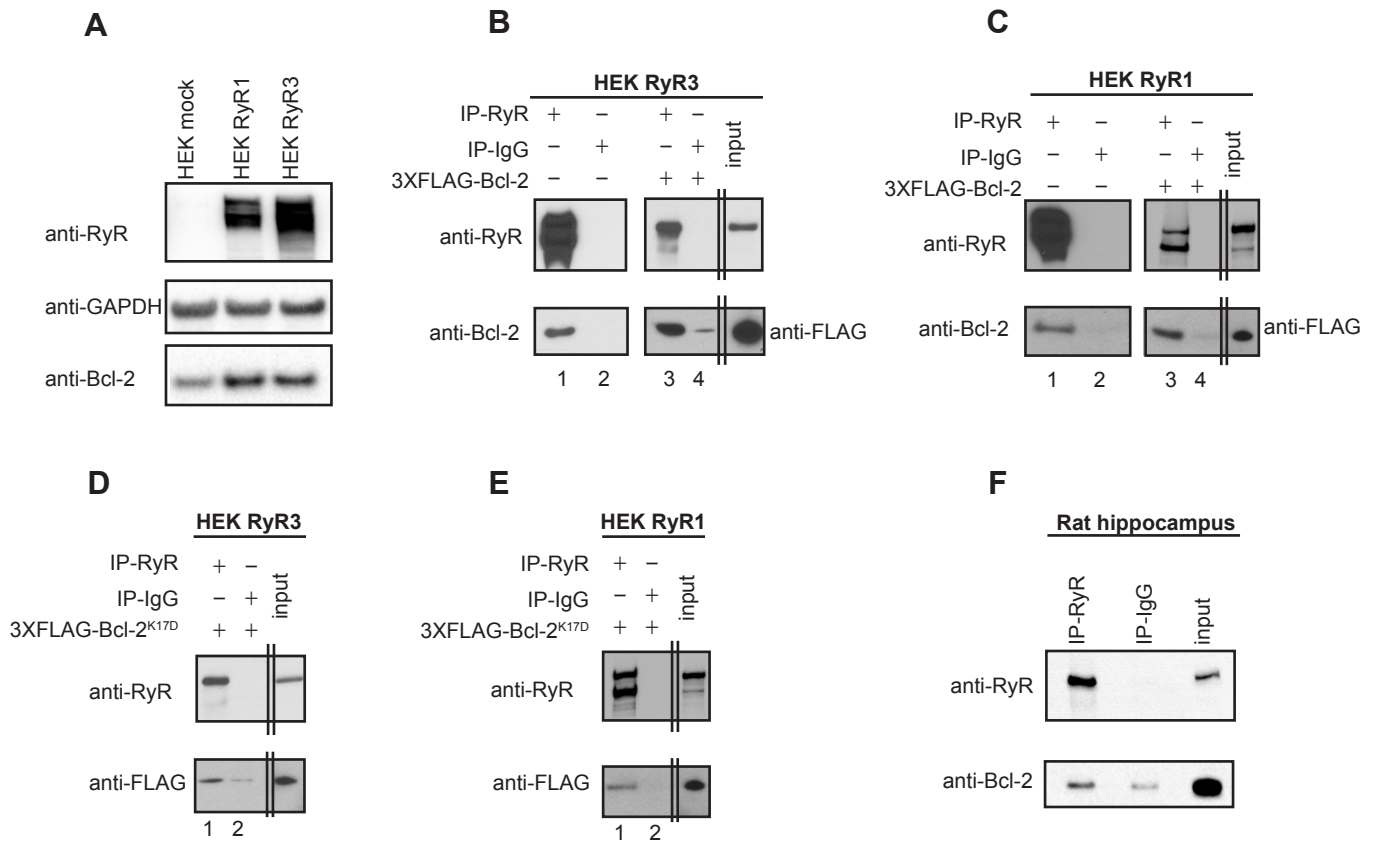


Figure 1

A

IP ₃ R1	(mouse)	1389	NVYTEIKC--NSLLPLDDIVRV	1408
IP ₃ R2	(mouse)	1390	NVYTEIKC--NSLLPLDDIVRV	1409
IP ₃ R3	(mouse)	1380	NVYTEIKC--TSLLPLEDVVTV	1399
RyR1	(rabbit)	2448	GEALRIRAILRSLVPLDDLVI	2469
RyR2	(rabbit)	2415	GEAIRIRSILRSLIPLGDLVGV	2436
RyR3	(mink)	2309	GEAIRIRSILRSLVPTEDLVI	2330

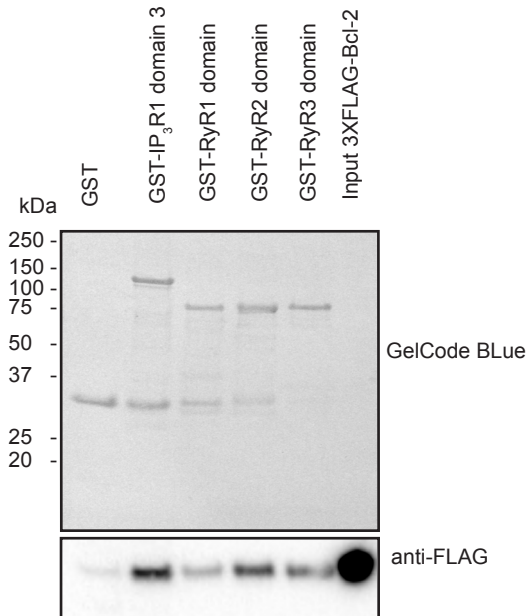
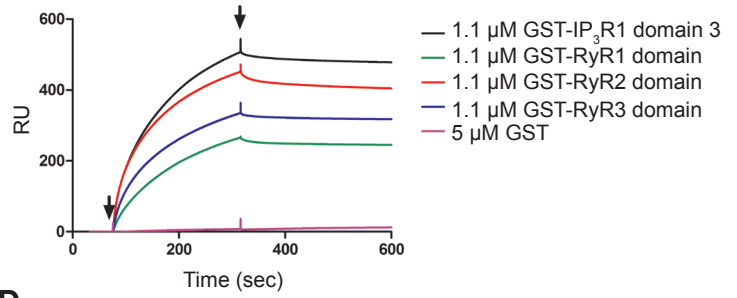
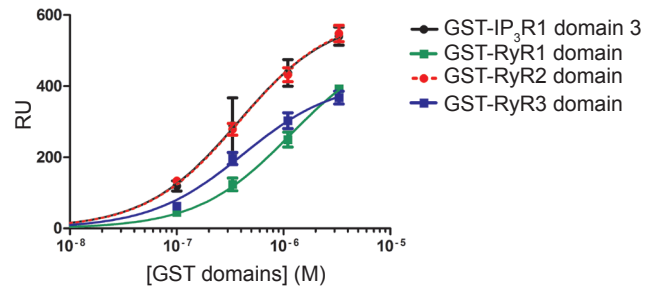
B**C****D**

Figure 2

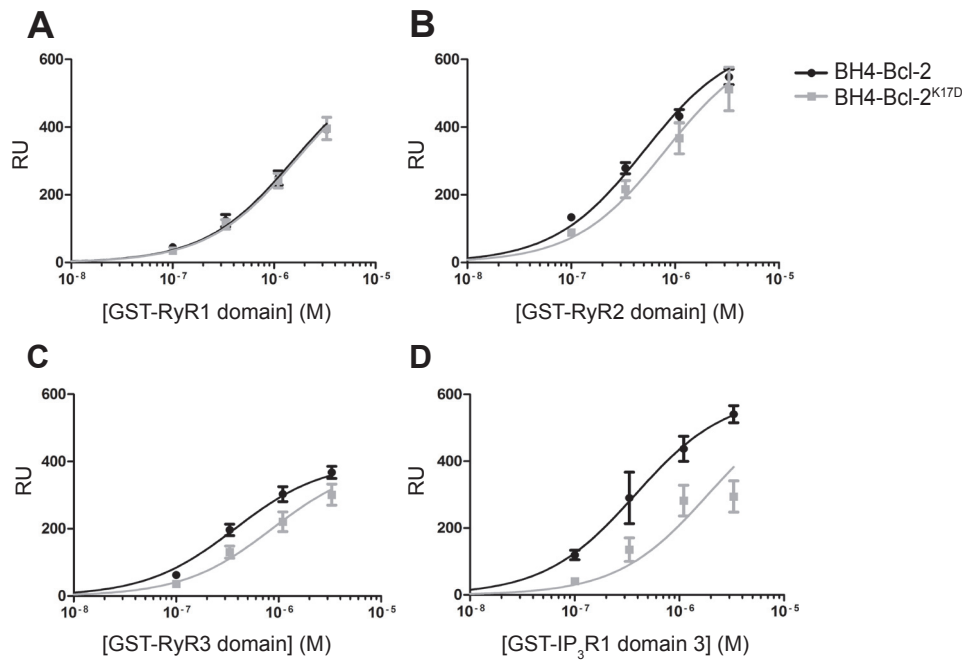


Figure 3

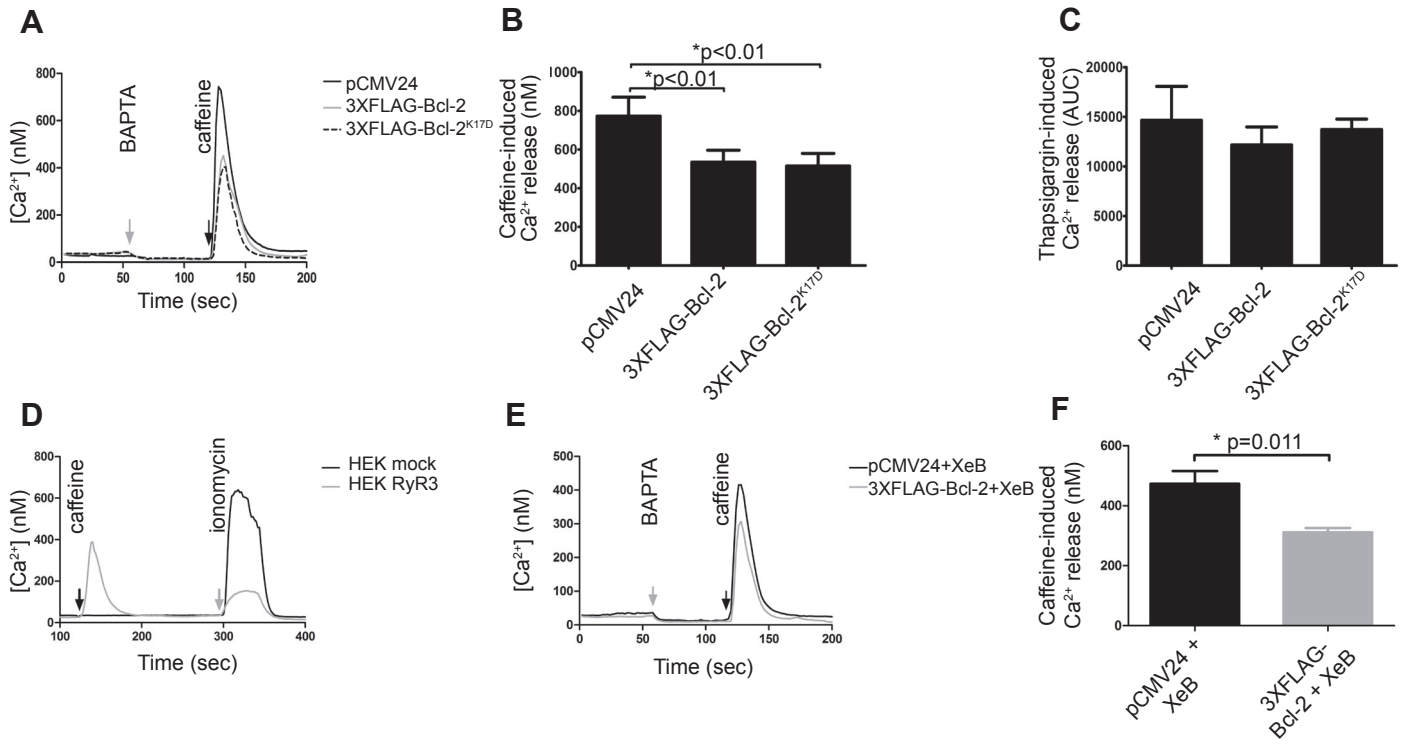


Figure 4

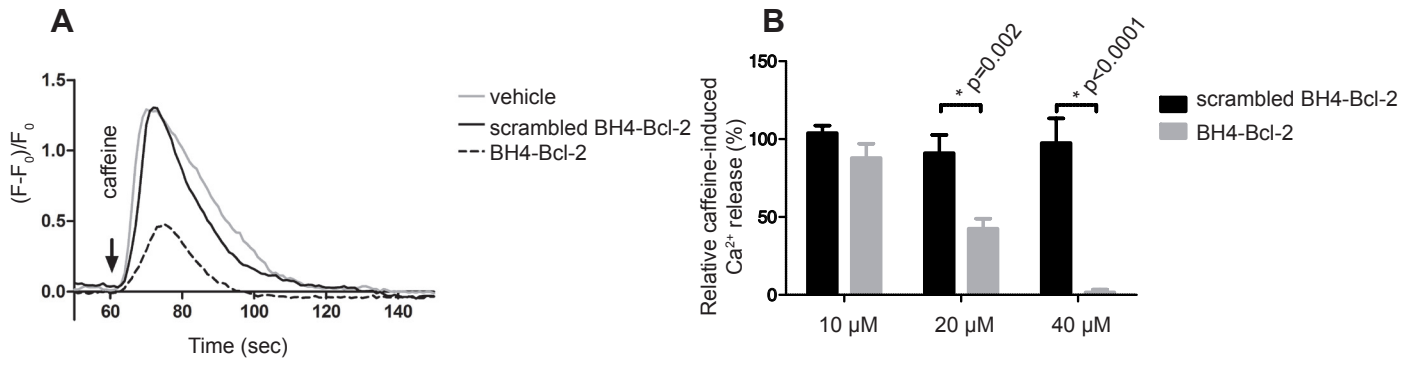


Figure 5

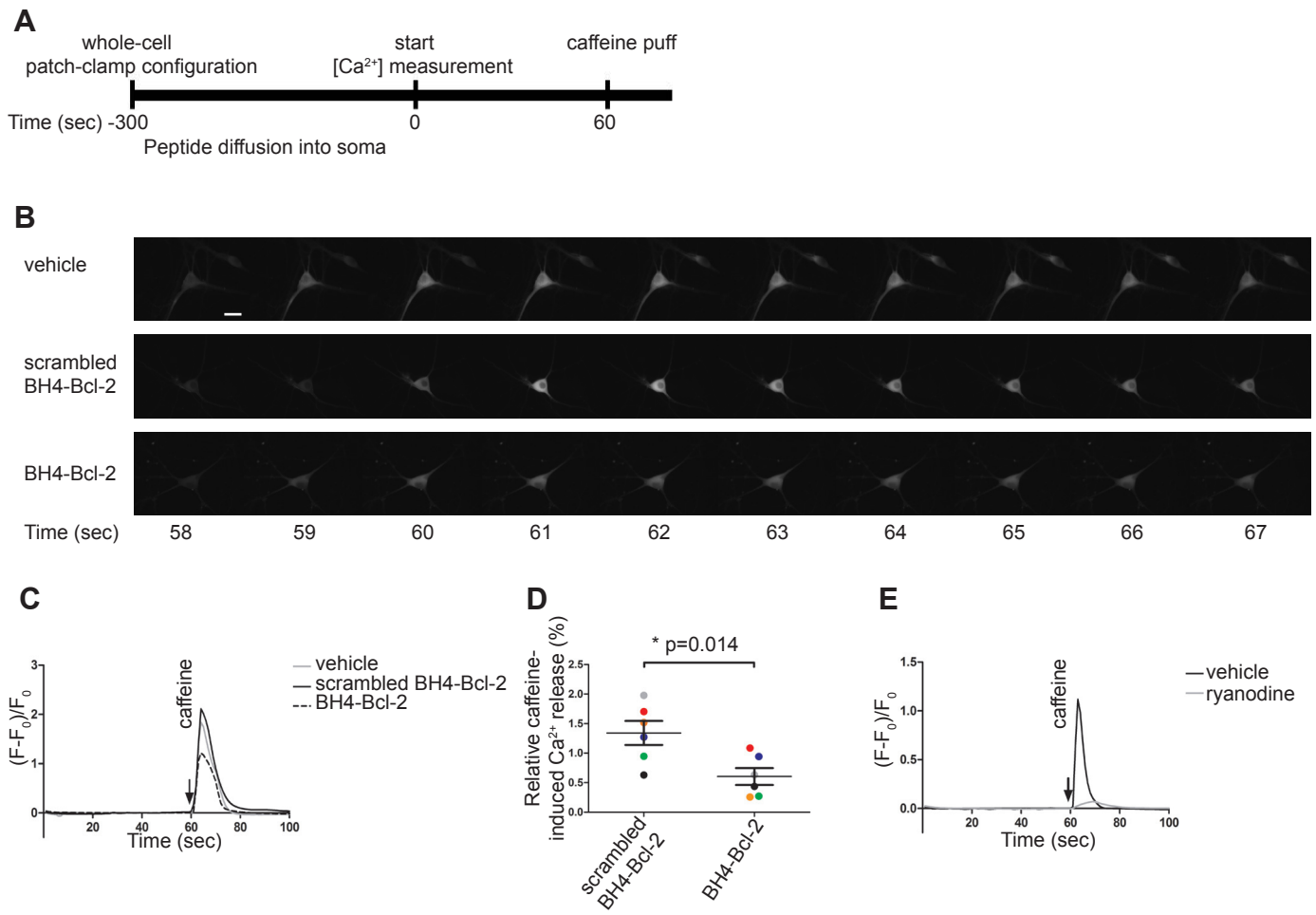
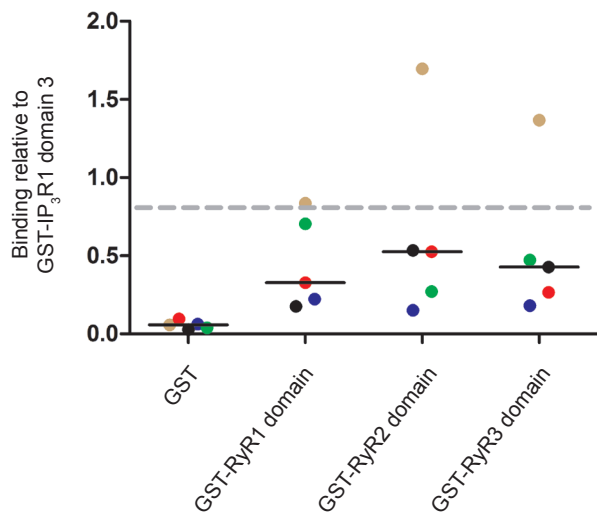


Figure 6

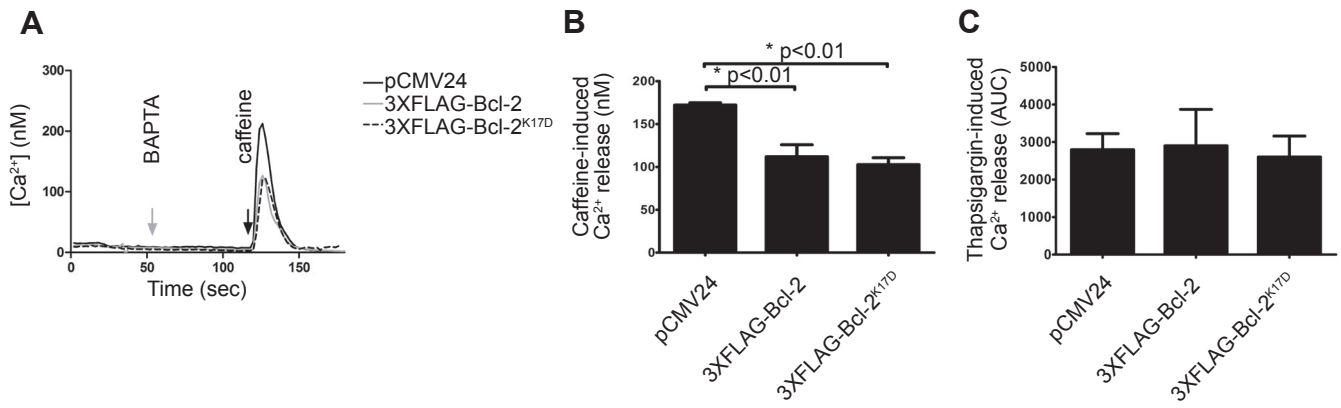
Table 1: Affinity of biotin-BH4-Bcl-2 and biotin-BH4-Bcl-2^{K17D} for the used GST-tagged IP₃R1 and RyR domains

	Approximate EC ₅₀ values (μM)	
	BH4	BH4 ^{K17D}
RyR1 domain	1.53	1.61
RyR2 domain	0.38	0.80
RyR3 domain	0.37	0.78
IP ₃ R1 domain 3	0.38	1.87

Approximated EC₅₀ values obtained from fitting using the Hill equation of the data presented in figure 3.



Quantification of the performed GST-pull downs. Each datapoint indicates binding of 3XFLAG-Bcl-2 to the indicated GST-domain normalized to the positive control, GST-IP₃R1 domain 3. Pull downs performed during the same experiment are indicated by the same color. All individual data points are given together with the median (horizontal bar) (n=5). The grey dashed line indicates the binding of 3XFLAG-Bcl-2 to the GST-IP₃R1 domain 3.



Fura-2 loaded, transfected (mCherry-positive) HEK RyR1 cells were selected for single-cell $[Ca^{2+}]$ measurements. (A) Average $[Ca^{2+}]$ traces (20 cells) from HEK RyR1 cells containing the pCMV24 vector, 3XFLAG-Bcl-2 or 3XFLAG-Bcl-2^{K17D} obtained in one experiment. The grey and black arrows respectively indicate the time points at which BAPTA (3 mM) or caffeine (4.5 mM) was administered. (B) Quantitative analysis of the caffeine responses in HEK RyR1 cells; values show averages \pm SEM of at least 3 independent experiments ($n > 80$ cells). (C) Quantitative analysis of ER Ca^{2+} -store content. The ER Ca^{2+} -store content was determined similarly as in panel A, except thapsigargin (1 μ M) was used instead of caffeine. The area under the curve (AUC) of the calibrated traces was used for determining the total ER Ca^{2+} -store content. The bar graph indicates the average AUC \pm SEM of at least 3 independent experiments ($n > 80$ cells) for each condition.